Program Digest, 2019 IEEE International Ultrasonics Symposium (IUS)
Glasgow, Scotland, October 6-9, 2019

Direction-independent bulk shear wave speed in 3D

A. Jorinde Kortenbout[1], Lana B.H. Keijzer[1], Nico de Jong [1, 2], Johan G. Bosch[1], Hendrik J. Vos[1, 2]

[1]Erasmus MC, University Medical Center Rotterdam, Department Thoraxcenter Biomedical Engineering, Rotterdam, the Netherlands
[2] Delft University of Technology, Faculty of Applied Sciences, ImPhys, Acoustical Wavefield Imaging, Delft, the Netherlands

***Abstract*— Natural shear waves in the neonatal brain potentially provide more information about mechanical properties of the brain in healthy and diseased state. Since these shear waves can be omnipresent, a direction-independent method to determine the propagation speeds of these shear waves is needed. In this study, we developed a direction-independent 3D wavenumber-frequency-domain technique to estimate the shear wave propagation speeds. Furthermore, a dominant propagation direction of the shear waves can potentially be determined with this technique. Measurements were performed in a homogeneous bulk phantom. The obtained results show a good agreement with the propagation speeds obtained with a Radon transform applied on 2D measurements and a clinical system with an elasticity mode.**

Keywords— Shear wave elastography; natural shear waves; f,k-domain; three-dimensional; neonatal brain

I. Introduction

Preterm neonates are born during a critical period of brain development. The preterm brain is extremely vulnerable and injuries during this phase may lead to long-term cognitive, motoric and behavioral problems [1]. Although the survival rate in preterm neonates has significantly improved in the last decade, neurodevelopmental problems are still very common [2, 3]. Adequate cerebral perfusion and oxygenation is essential for normal brain development. Therefore, objective monitoring of the brain and its perfusion is necessary for early diagnosis and treatment of brain injury during this critical period of brain development. Techniques that are currently used for neuroimaging, such as MRI, CT or PET, require transportation of the patient, use ionizing radiation and/or are expensive. Therefore, these methods are not suited for neuromonitoring of the critically ill and/or very preterm neonates. Ultrasound imaging of the neonatal brain through the anterior fontanel is possible at the patient's bedside, is non-invasive, radiation free and is considered to be a safe technique. Ultrasound is already used for evaluation of the neonatal brain anatomy and for detection of brain injury in the neonatal intensive care unit [4].

Perfusion changes, edema and changes in intracranial pressure may provoke brain injury. Furthermore, these changes might influence the stiffness of the brain [5]. Shear wave elastography (SWE) can be used to measure tissue stiffness. It might potentially provide a quantitative measure of brain tissue condition and enhance the diagnostic sensitivity of conventional ultrasound [5]. For ultrasound SWE, the shear wave propagation speed is measured, which is directly related to the Young's modulus, characterizing the tissue stiffness [6]. In first reports of this technique in neonates, Albayrak and Kasap [7] and Su et al. [8] both found different SW speeds for different parts of the neonatal brain. Lower propagation speeds were measured for an immature neonatal brain than for a term neonatal brain. Furthermore, deCampo and Hwang [5] used SWE to measure brain injury in neonates.

In these studies, shear waves were induced with acoustic radiation force (ARF). However, the safety and efficacy of repeated use of ARF has never been tested in neonatal brain imaging. Since we aim at SWE to monitor neonatal brain elasticity with repeated measurements over the first few days after birth, ARF might not be the preferred technique. Therefore, we investigate the 'passive' echographic detection of natural shear waves in the brain with subsequent shear wave analysis. These natural shear waves are assumed to be induced by arterial pulsations and/or cerebrospinal fluid exchange [9]. Since these shear waves might be omnipresent and/or arise from an unknown location, a direction-independent method is necessary to measure these SWs. In this study, we investigate such a method. We developed a 3D technique in the wavenumber-frequency domain to estimate SW speed with a global, direction- and user- independent method. We tested the technique in a bulk phantom by recording multiple 2D SW measurements, to capture the 3D shear wave field.

II. Method and Materials

A. Phantom

A cylinder-shaped, homogeneous and isotropic phantom (diameter 10 cm, height 6.5 cm) was created by 1 cycle of freeze-thawing 10% polyvinyl alcohol powder, 1% silicon carbide powder (50% SiC K-800, MTN-Giethoorn, NL, 50% SiC K-400 Cats Hoogvliet, NL), 20% ethylene glycol (density 1,11 g/mol , Boom BV Meppel, NL) and 69% distilled water.

B. Measurement set-up

The phantom was placed in a water tank. A Zonare ZS3 system (Mindray, San Jose, CA) with a P4-1c probe was used for acquiring IQ-data with a custom high frame rate (HFR, 1000 Hz) mode. To induce reproducible mechanical waves, a metal rod attached to an electromagnet produced a downwards-oriented tap on a metal rod glued into the phantom. As shown in Fig.1A, this rod covered the entire thickness of the phantom to exert the force of the tap over the entire phantom. The ultrasound probe was attached to a rotating turntable with protractor, which allowed for rotating the probe with an accuracy of a few degrees.

This research is part of the project 'Monitoring infant brain perfusion by trans-fontanel echography (MIFFY)' with project number 15293, which is (partly) financed by the Netherlands Organization for Scientific Research (NWO).

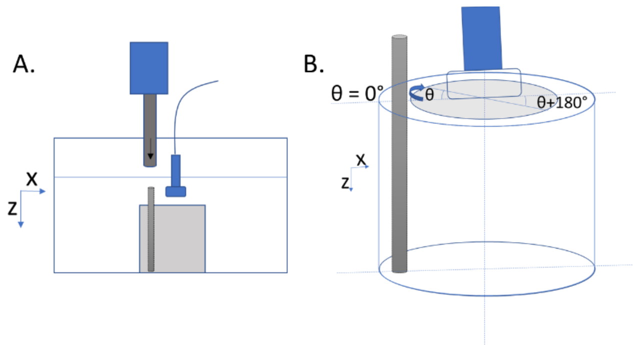

Fig. 1. A: Schematic overview of the measurement set-up. The phantom is placed in a watertank. A metal rod attached to an electromagnet can produce a downwards-oriented tap on the rod in the phantom, B: Schematic overview of the phantom with rotating turntable, where θ is the rotation angle of the probe.

First, the probe was visually aligned with the metal rod, such that the field imaged by the probe (θ = 0°) was in line with the metal rod, and an HFR measurement was performed. Subsequently, the probe was rotated around its central axis with steps of 5 degrees, as illustrated in Fig. 1B. In total, 36 2D ultrasound measurements were performed.

For comparison of our technique with a more clinically accepted method, we also performed SWE measurement with a SuperSonic Imagine (SSI) Aixplorer (Aix-en-Provence, France) [10].

C. Data analysis

A one-lag autocorrelation technique was applied to the IQ data to obtain axial tissue velocities [11]. All 36 measurements were synchronized in time by cross correlation of the time signal of the central point on the rotation axis in each 2D image plane. The time shift found was used to match the 2D sequences in time assuring that the push occurred at the same moment. Since the probe was rotated over θ along its central axis, each acquisition was vertically split into two separate measurements for θ and (θ+180), respectively. After this, we obtained 72 2D datasets covering the whole 360° cylindrical space. The Tissue Doppler Imaging (TDI) data were then interpolated to a 3D Cartesian domain.

A temporal Fourier transform was performed on the 3D Cartesian TDI dataset. For every frequency component ($df = 10$ Hz), a 3D spatial Fourier transform was performed to obtain data in 3D k-space (k_x, k_y, k_z). Independent of the actual spatial direction of the SWs propagating with a certain SW speed C_s, the maximum intensity of energy is expected to be located on a sphere with radius $|k_S|$,

$$|k_s| = \frac{f}{C_s} \qquad (1)$$

where we neglect the 2π for clarity of equations. Since the phantom was assumed to be homogeneous and isotropic, the value of $|k_S|$ was determined by remapping the measurement data from the k_x, k_y, k_z domain onto a single scalar axis $|\vec{k}|$,

$$|\vec{k}| = \sqrt{{k_x}^2 + {k_y}^2 + {k_z}^2} \qquad (2)$$

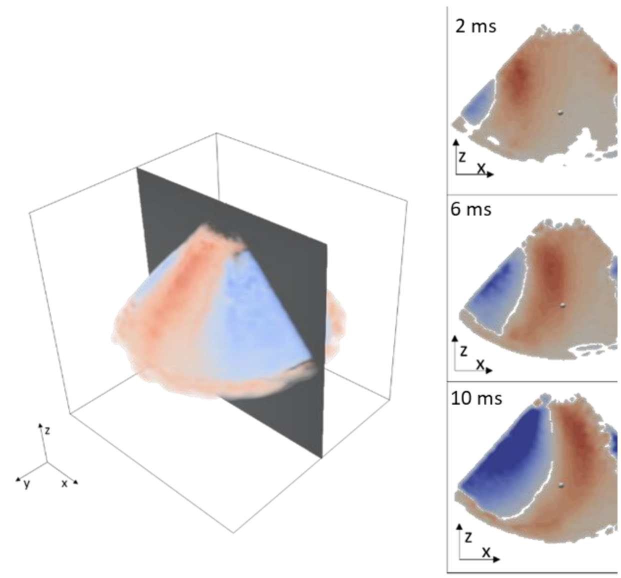

Fig. 2. Interpolated 3D TDI dataset for the situation with the SW source in line with the imaged field of the probe (θ=0°). A SW propagating from left to right is shown in the inserts, depicting 2D measurements at 3 different time points for θ=0°.

The value of $|k_S|$ now corresponds to the peak of the data cloud in this remapped format, where the peak is found by a straightforward global peak searching algorithm. SW speed C_s was calculated by inverting (1),

$$C_S = \frac{f}{|k_S|} \qquad (3)$$

The major frequency components of the SW were measured to lie within the range of 30 to 150 Hz. We used linear regression to further improve robustness in SW speed estimation. This linear regression was performed over the $|k_S|$ values for all values of f in the range of 30-150 Hz. The SW-speed was subsequently determined by calculating the slope of the regression line.

The individual 2D TDI measurements were also separately analyzed with a more conventional space-time domain technique. In this analysis, the TDI data were bandpass filtered with a 6th order Butterworth filter between 30 and 150 Hz. The SW speed was determined by applying a Radon transform [12]. It is expected that when there is an angular misalignment θ between the 2D image plane and the wave propagation path, the measured SW speed will have a 1/cos(θ) overestimation. Thus, the apparent propagation speed is always larger than the actual SW speed [12]. The SW was laterally tracked with a Radon transform at 10 depths.

III. Results

Fig. 2 shows the interpolated 3D TDI dataset for θ=0° and a cross section at 3 different time points, where the SW is propagating from left to right.

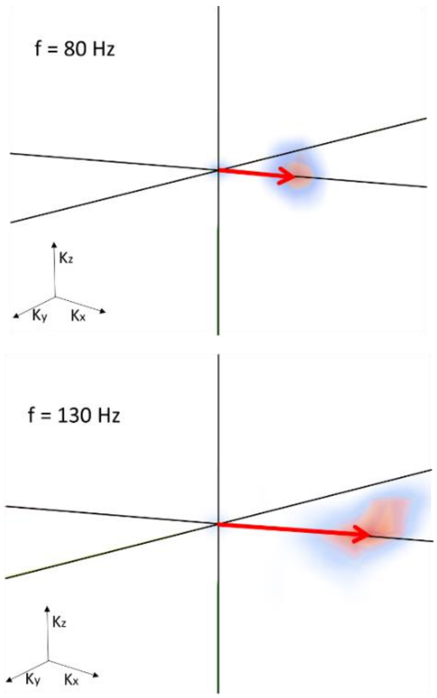

Fig. 3. k- space at 80 Hz and 130 Hz. For both frequencies, the highest energy was found in the k_x direction. The red arrows depict |k|. The wavenumber was found to increase with a factor of 2 for f=130 Hz compared to 80 Hz.

Fig. 3 depicts the k-space for two different frequencies, where the maximum intensity is located at the k_x axis for both frequencies. A larger $|k_S|$ value (i.e., the length of the red vector) was found for higher frequencies. Fig. 4 shows the $|k_S|$ values found for the frequency range of interest by selecting the maximum intensities in |k|-space. As expected, the value of $|k_S|$ generally increases with increasing frequency.

The results of the linear regression to improve the robustness of the propagation speed estimate is shown in Fig. 4. The linear regression estimate was y = 0.28x ($R^2 = 0.89$). The speed was calculated by finding the slope of the linear regression estimate and was 3.6 ± 0.6 m/s.

The SW speed was separately estimated for the individual 2D measurements by tracking the SW with a Radon transform, see Fig. 5. In the aligned plane, the mean shear wave speed was found to be 3.5 ± 0.3 m/s. As expected, the SW speed was found to increase with the misalignment between the SW propagation direction and the imaged field of view with a factor of roughly 1/cos(θ) for θ below 35°. For higher θ, the overestimation becomes larger, which might be explained by deviation from the underlying assumption that the shear wave is planar in 3D.

The SW speed measured with the SSI Aixplorer was 3.8 ± 0.06 m/s.

IV. Discussion

We obtained comparable propagation speeds with the proposed 3D wavenumber-frequency technique, a Radon transform applied to a 2D plane aligned with the SW source, and the SWE measurements performed with the SSI Aixplorer. The 3D wavenumber-frequency technique has multiple advantages.

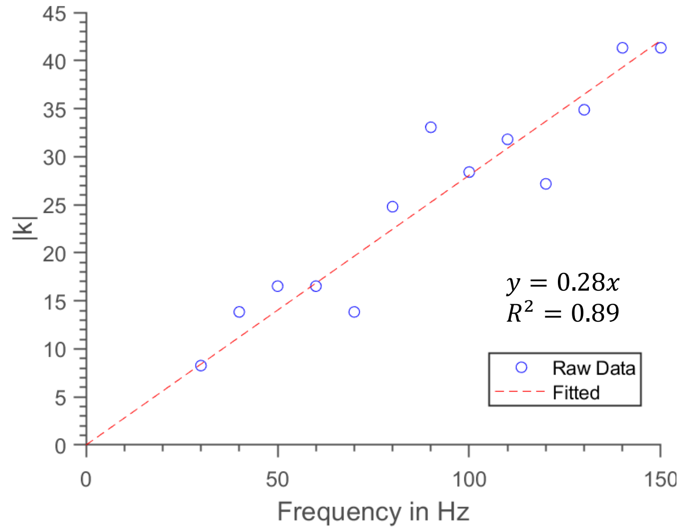

Fig 4. $|k_S|$ was found to generally increase with frequency. The blue points indicate the $|k_S|$ values corresponding to the maximum intensity in wavenumber-frequency domain at different frequencies between 30 and 150 Hz. The red line indicates the linear regression estimate.

First, the location of the SW source does not have to be known. This could be an advantage for natural SWE measurements. As expected, we found an overestimation in propagation speed for 2D measurements having a misalignment between the probe and the SW source. Second, the proposed 3D technique is direction-independent and therefore misalignment issues are avoided. In a preliminary simulation (data not shown), we found correct SW speed values when using multiple SW sources at different locations. A future phantom experiment with omnidirectional SW sources could further investigate whether the correct SW speed can also be extracted experimentally. Third, the dominant SW propagation direction could be determined by using the 3D technique. The main SW propagation direction can be found by selecting the vector in k-space pointing to the maximum value. In this study, these vectors were found to be in the k_x-direction, indicating that the SW mainly propagated in the x-direction, as shown in Fig. 3.

In the presented study, a bulk, uniform, homogeneous phantom was used. However, for more complex in vivo situations, the average propagation speed can probably still be determined by using the remapped measurement data $|\vec{k}|$. For anisotropic situations, propagation speeds in different directions can be obtained by selecting separated k-wave directions, instead of remapping the entire dataset to a single $|\vec{k}|$ value. To estimate local SW speed values in inhomogeneous media, smaller blocks for k-space analysis should be selected. However, the maximum spatial resolution of local SW speed values by using the proposed 3D technique should be further investigated.

Whether natural SWE is possible in the neonatal brain is still unknown. Zorgani et al. [9] looked at natural SWs of the adult brain with MRI. They used time reversal techniques to extract information from the complex natural SW field [13]. However, since MRI was used, the framerate was not high enough for measuring SW speeds. Instead, the SW wavelength was

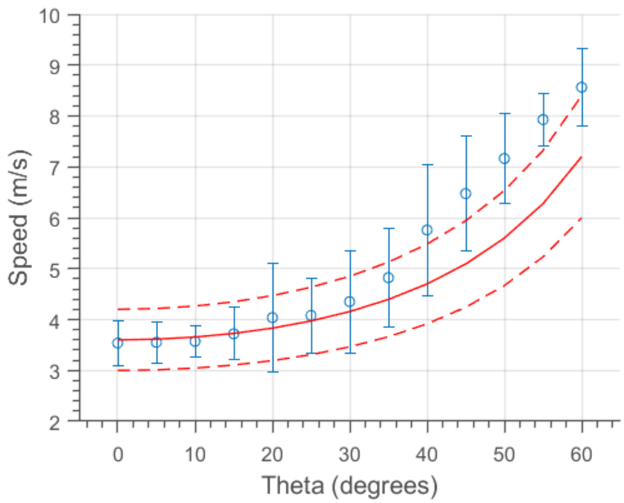

Fig. 5. Mean and standard deviation of the shear wave speed values in blue obtained for the individual 2D measurement by applying a Radon transform. Shear wave propagation speeds were found to increase with misalignment between SW propagation direction and the imaged field of view. The red (dashed) line indicates the SW speed (and standard deviation) by k-space estimation (3.6±0.6), with an $1/\cos(\theta)$ factor applied per angle for comparison to the Radon-based SW speeds.

extracted at multiple locations in the brain [9, 13]. This study indicates the presence of a complex natural SW field in the brain, which can potentially also be measured with ultrasound in the neonatal brain. Our next step will be to explore this.

V. Conclusion

This study shows the preliminary results of a 3D wavenumber-frequency-domain technique to measure global SW speed in a bulk phantom with a-priori unknown wave source and wave propagation directions. A good agreement was found between this method, a clinical system with a SWE mode, and the Radon transform applied on 2D measurements. Moreover, any dominant propagation direction of the SW could be determined with this 3D technique.

Acknowledgement

We thank dr. G. Mclaughlin and dr. Y. Chen of Mindray Innovation Center (San Jose, California) for the use of the Zonare ultrasound system and the high frame rate mode.

References

[1] G. P. Aylward, "Neurodevelopmental Outcomes of Infants Born Prematurely," Journal of Developmental & Behavioral Pediatrics, vol. 35, pp. 394-407, 2014.

[2] J. J. Volpe, "Brain injury in premature infants: a complex amalgam of destructive and developmental disturbances," The Lancet Neurology, vol. 8, pp. 110-124, 2009.

[3] B. J. Stoll, N. I. Hansen, E. F. Bell, M. C. Walsh, W. A. Carlo, S. Shankaran, et al., "Trends in Care, Morbidity, and Mortality of Extremely Preterm Neonates," JAMA, vol. 314, pp. 1039-1051, 2015.

[4] A. Plaisier, M. M. Raets, G. M. Ecury-Goossen, P. Govaert, M. Feijen-Roon, I. K. Reiss, et al., "Serial cranial ultrasonography or early MRI for detecting preterm brain injury?," Arch Dis Child Fetal Neonatal Ed, vol. 100, pp. F293-300, 2015.

[5] D. deCampo and M. Hwang, "Characterizing the Neonatal Brain With Ultrasound Elastography," Pediatric Neurology, vol. 86, pp. 19-26, 2018.

[6] J. L. Gennisson, T. Deffieux, M. Fink, and M. Tanter, "Ultrasound elastography: principles and techniques," Diagn Interv Imaging, vol. 94, pp. 487-95, 2013.

[7] E. Albayrak and T. Kasap, "Evaluation of Neonatal Brain Parenchyma Using 2-Dimensional Shear Wave Elastography," J Ultrasound Med, vol. 37, pp. 959-967, 2018.

[8] Y. Su, J. Ma, L. Du, J. Xia, Y. Wu, X. Jia, et al., "Application of acoustic radiation force impulse imaging (ARFI) in quantitative evaluation of neonatal brain development," Clin Exp Obstet Gynecol, vol. 42, pp. 797-800, 2015.

[9] A. Zorgani, R. Souchon, A. H. Dinh, J. Y. Chapelon, J. M. Menager, S. Lounis, et al., "Brain palpation from physiological vibrations using MRI," Proc Natl Acad Sci U S A, vol. 112, pp. 12917-21, 2015.

[10] J. Bercoff, M. Tanter, and M. Fink, "Supersonic shear imaging: a new technique for soft tissue elasticity mapping," IEEE Trans Ultrason Ferroelectr Freq Control, vol. 51, pp. 396-409, 2004.

[11] B. Brekke, L. C. L. Nilsen, J. Lund, H. Torp, T. Bjastad, B. H. Amundsen, et al., "Ultra-high Frame Rate Tissue Doppler Imaging," Ultrasound in Medicine & Biology, vol. 40, pp. 222-231, 2014.

[12] H. J. Vos, B. M. van Dalen, I. Heinonen, J. G. Bosch, O. Sorop, D. J. Duncker, et al., "Cardiac Shear Wave Velocity Detection in the Porcine Heart," Ultrasound in Medicine & Biology, vol. 43, pp. 753-764, 2017.

[13] S. Catheline, R. Souchon, M. Rupin, J. Brum, A. H. Dinh, and J.-Y. Chapelon, "Tomography from diffuse waves: Passive shear wave imaging using low frame rate scanners," Applied Physics Letters, vol. 103, p. 014101, 2013.